Desalination and Water Treatment
www.deswater.com

doi:10.5004/dwt.2018.22461

115 (2018) 172–180
May

Synthesis of iron-doped Bi_2WO_6 high-performance visible-light-induced photo catalyst by a single-step solvo thermal process

Chung-Hsin Wu[a,*], Chao-Yin Kuo[b], Tai-Jyun Chang[a]

[a]*Department of Chemical and Materials Engineering, National Kaohsiung University of Science and Technology, 415 Chien Kung Road, Kaohsiung, Taiwan, Tel. 886-7-3814526, Fax 886-7-3830674, email: wuch@nkust.edu.tw (C.-H. Wu), Tel. 886-958352592 email: as62398@yahoo.com.tw (T.-J. Chang),*
[b]*Department of Environmental and Safety Engineering, National Yunlin University of Science and Technology, Yunlin, Taiwan, Tel. 88655347311, email: kuocyr@ms35.hinet.net (C.-Y. Kuo)*

Received 2 February 2018; Accepted 4 May 2018

ABSTRACT

In this study, iron-doped Bi_2WO_6 (FeBWs) photo catalyst was synthesized by a single-step solvo thermal process. Fe/W molar ratios of 0.1–10 were used. The surface characteristics of the prepared FeBWs were analyzed by X-ray diffractometry (XRD), Fourier transform infrared spectroscopy (FTIR), scanning electron microscopy, transmission electron microscopy, specific surface area analysis, UV-Vis spectrophotometry, fluorescence spectrophotometry and X-ray photo electron spectroscopy. The photo catalytic activities of FeBWs were compared using the decolorization of C.I. Reactive Red 2 (RR2) with solar-light photo catalysis and visible-light photo catalysis. No XRD peaks of iron metal or iron oxide were detected, possibly because iron ions were doped into the lattice of Bi_2WO_6. The results of FTIR revealed that some iron ions substituted Bi^{3+} in FeBWs. Iron doping into Bi_2WO_6 reduced the band gap from 3.1 to 1.3 eV. All prepared FeBWs were visible-light-induced photo catalysts. The optimal Fe/W molar ratio was 5 and solar-light photo catalysis increased the RR2 decolorization rate from 3.34 h^{-1} (Bi_2WO_6) to 8.48 h^{-1} (FeBWs) while visible-light photo catalysis increased it from 0.11 h^{-1} to 7.36 h^{-1}. The doping of iron ions into Bi_2WO_6 increased the separation of photo generated electron-hole pairs by acting as traps and increased photo catalytic performance. The photo generated holes and super oxide radicals were the major active species in FeBW photo catalysts.

Keywords: Bi_2WO_6; Visible-light; Solvo thermal; Iron ion, Photo catalysis

1. Introduction

Bi_2WO_6 (BW) is one of the simplest members of the Aurivillius oxide family (when n = 1) of layered perovskites with the general formula $Bi_2A_{n-1}B_nO_{3n+3}$ (A = Ca, Sr, Ba, Pb, Na, K; B = Ti, Nb, Ta, Mo, W, Fe; and n = number of perovskite-like layers $(A_{n-1}B_nO_{3n+1})^{2-}$). Their structures are composed of alternating perovskite-like and fluorite-like blocks [1]. BW is a new type of visible-light-induced photo catalyst; it is stable and non-toxic and it does not cause secondary pollution. BW has potential as a novel photo catalyst; however, its high rate of recombination of photo generated electron-hole pairs causes it to has a low photo quantum efficiency, resulting in low photo catalytic performance, so its application remains limited. In a perovskite structure, not only can the number of A and B sites vary, but also a combination of cations can be incorporated at the A and/or B sites to form substituted perovskites. These variations can change the electronic structure, affecting the optical, electrical and photo catalytic properties [2].

Much effort has been made to develop visible-light-induced photo catalysts. Current photo catalysts have critical shortcomings such as the short lifetime of the photo generated electron-hole pairs and the insufficient absorption of visible-light, which limit their application. The most popular method for tuning the absorption edge of a photo catalyst is to dope the host materials with foreign species.

*Corresponding author.

1944-3994 / 1944-3986 © 2018 Desalination Publications. All rights reserved.

The general effects of doping a photo catalyst include the introduction of an impurity energy level, enhancement of the adsorption in the visible-light region, an increase in the number of active sites, and the suppression of photo generated electron-hole recombination.

To improve the separation of photo generated electron-hole pairs, many researchers loaded BW with metal ions, such as Fe [3, 4], Cu [5], Eu [6], Zr [7], Ba [8], Ag [9] and Mo [10]. Modification using transition metals is a frequent topic of photo catalytic study, and its purpose to improve photo catalytic activity was by trapping electron-hole pairs. Tan et al. [5] found that Cu loading effectively narrows the band gap of BW and that significantly improves the photo catalytic activities of BW. Li et al. [8] revealed that the doping of Ba into BW increases its specific surface area, reduces its crystalline size, provides electron traps and facilitates the separation of photo generated electron-hole pairs. Zhang et al. [7] showed that doping zirconium into BW effectively inhibited the recombination of photo generated charge carriers. Previous investigations have demonstrated that doping Fe, Cu, Eu, Zr, Ba, Mo or Ag into BW efficiently improves it photo catalytic ability [3–10].

Fe salts are low-cost and nontoxic. Fe^{3+} has been extensively used in the doping of photo catalyst owing to its half-filled electronic configuration [11]. Doping of Fe into the substitutional sites of $BiVO_4$ effectively improved the migration and separation of photo generated carriers and increased the utilization of visible-light [12]. Guo et al. [3] and Sriwichai et al. [4] both reported that the loading BW with iron ions increased its photo catalytic performance under visible-light. However, all of the cation doping into BW in the literature is conducted using the hydrothermal method, except for that by Dumrongrojthanath et al. [9], who doped Ag into BW using a solvo thermal process. Furthermore, all doping Fe/W molar ratios in Fe-doped BW were very low (0.0018%–2%), but coupling Fe_2O_3 [13] (best at Fe/W molar ratio 0.8) or Fe_3O_4 [14] (best at Fe/W molar ratio 1.3) with BW yielded the best performance at a high Fe/W molar ratio. To the best of our knowledge, the use of the solvo thermal method to synthesize the iron ion-doped BW composites (FeBWs) has not been studied. Accordingly, in this investigation, ethylene glycol (EG) was used as a solvent in the synthesis of FeBWs. The photo catalytic activity of the prepared FeBWs in the photo catalysis of C.I. Reactive Red 2 (RR2) was evaluated. The goals of this investigation were (i) to determine the effects of the Fe/W molar ratio on the photo catalytic activity of FeBWs under solar-light and visible-light; (ii) to measure the surface characteristics of prepared FeBWs; and (iii) to identify the reusability and major oxidative species in the FeBWs system.

2. Materials and methods

2.1. Materials

All chemicals were reagent-grade and used as received without further purification. Bismuth(III) nitrate ($Bi(NO_3)_3{\cdot}5H_2O$), sodium tungstate ($Na_2WO_4{\cdot}2H_2O$) and iron(III) nitrate ($Fe(NO_3)_3{\cdot}9H_2O$) were used as precursors in the formation of Bi, W and Fe, respectively, which were used to generate FeBWs (Katayama, Japan). RR2 ($C_{19}H_{10}Cl_2N_6Na_2O_7S_2$) was purchased from Sigma Aldrich (USA). Sodium nitrite ($NaNO_2$) and EG; both were obtained from Katayama, were used as an ultra violent-light cut-off agent and as a solvent in the solvo thermal process, respectively. To detect the active species that formed in the FeBW system, hydroxyl radicals, holes and super oxide radicals were quantified by adding isopropanol (IPA) (J.T. Baker, USA), ethylenediaminetetraacetic acid disodium salt (EDTA-2Na) (Katayama) and K_2CrO_4 (Katayama), respectively. The pH of the solution was adjusted by adding 0.1 M HNO_3 or NaOH during the reaction, both of which were purchased from Merck (USA).

2.2. Preparations of FeBWs

BW was prepared under conditions that Wu et al. [15] identified as optimal. A 3.881g of bismuth(III) nitrate, 1.319 g sodium tungstate and the desired amount of iron(III) nitrate (0.1616, 0.404, 0.808, 1.616, 3.232, 8.08 or 16.16 g) were added to 70 mL EG and the resulting solution was vigorously magnetically stirred, yielding Fe/W molar ratios of 0.1, 0.25, 0.5, 1, 2, 5 and 10. The mixtures were adjusted to pH 2 by adding 10 M NaOH with stirring for 1 h. The mixtures were sealed in a 100 mL Teflon-lined stainless steel autoclave and heated at 433 K under self-generated pressure for 12 h; they then cooled naturally to room temperature. The precipitates were collected by filtration and washed using 50 mL 95% ethanol and 100 mL D.I. water to remove any residual impurities. The samples were finally dried in air at 333 K for 24 h. The samples with Fe/W molar ratios of 0.1, 0.25, 0.5, 1, 2, 5 and 10 were denoted as 0.1FeBW, 0.25FeBW, 0.5FeBW, 1FeBW, 2FeBW, 5FeBW and 10FeBW, respectively.

2.3. Characterization of prepared FeBWs

The phase structure of FeBWs was analyzed using an X-ray diffractometer (Bruker D8 SSS, Germany) with CuKα radiation (40 kV, 30 mA) over the 2θ range of 15°–75°. The distinctive functional groups of FeBWs were investigated using Fourier transform infrared spectroscopy (FTIR). A Perkin-Elmer spectrometer (One Nicolet Avatar 370, Japan) was used to obtain FTIR absorption spectra in the region of 400–4000 cm^{-1}. Diffuse reflectance ultra violent (UV)-visible (Vis) spectra of FeBWs, obtained using a UV-Vis spectrophotometer (JAS.CO-V670, Japan), were used to calculate the bandgap. The morphology and micro structure of the FeBWs were characterized by scanning electron microscopy (SEM) (JEOL 6330 TF, Japan) and transmission electron microscopy (TEM) (JEOL 3010, Japan). The photoluminescence (PL) spectra were used to examine the efficiency of charge carrier transfer and separation because PL emission is caused by the recombination of photo generated electron-hole pairs. The PL spectra of FeBWs were obtained at room temperature using a fluorescence spectrometer (Hitachi F-4500, Japan) with an excitation wavelength of 300 nm from a xenon lamp. The Brunauer-Emmett-Teller (BET) specific surface area of FeBWs was obtained using a Micro meritics ASAP 2020 system (USA). X-ray photo electron spectroscopic (XPS) measurements were made using a PHI Quantum 5000 XPS system (USA) with a monochromatic Al Kα source and a charge neutralizer. Binding energies were calibrated relative to the C_{1s} peak at 284.6 eV.

2.4. Photo catalysis experiments

The RR2 concentration, photo catalyst dosage and temperature in all of the experiments were 20 mg/L, 0.5 g/L and 298 K, respectively. Photo catalysis experiments were performed in a 3 L glass reactor. A 400 W Xe lamp (200 nm < wavelength < 700 nm, UniVex BT-580, Taiwan) was used to provide simulated solar-light radiation. The intensity of the light from the lamp was 30.3 mW/cm^2. A quartz appliance that was filled with 2 M $NaNO_2$ solution was placed on the top of the reactor to cut the UV and to provide visible-light [16]. Adsorption experiments were conducted in darkness. The reaction medium was stirred continuously at 300 rpm and aerated with air to maintain a suspension. Following sampling at specific intervals, solids were separated by filtration through a 0.22 μm filter (Millipore, USA), and the RR2 that remained in the filtrate was analyzed by measuring its absorbance at 538 nm using a spectrophotometer (Hitachi U-5100, Japan). To evaluate the reusability of 5FeBW, used 5FeBW powder was recovered by filtration through a 0.22 μm filter. The recovered 5FeBW powder was used in the subsequent photo catalytic run without any washing. Some experiments were performed in triplicate and mean values were reported.

3. Results and discussion

3.1. Surface characteristics of FeBWs

The XRD patterns in Fig. 1 display the phase structure and the phase composition of BW and FeBWs, which reveal the effects of the iron doping concentration on the phase structure of BW. The peaks at 28.3°, 32.8°, 47.0° and 55.8° correspond to the (1 1 3), (2 0 0), (0 2 6) and (3 1 3) reflections of the crystal phases, respectively; the distinct diffraction peaks correspond to the orthorhombic BW phase (JCPDs no. 73-1126). As the iron doping concentration increased, the breadth of the diffraction peaks increased and their intensities decreased. The broad diffraction peaks implied that iron doping inhibited grain growth [17,18]. The broad diffraction peaks indicated that Fe^{3+} ion doping restrained grain growth and the formation of smaller BW crystallites, potentially increasing the number of lattice defects. The ionic radius of Fe^{3+} (0.064 nm) [3,19,20] is much smaller than that of Bi^{3+} (0.103 nm) [6,21] but close to that of W^{6+} (0.062 nm) [5,7]. The peak shift is attributable to the lattice expansion that is caused by the incorporation of a small proportion of iron atoms [12] and the substitution of W^{6+} by Fe^{3+}. Loading with iron ions inhibited the growth of the crystal phase of BW, as did the doping of BW with goethite [22]. In Cu-doped BW, when the content of Cu increased to 10%, the monoclinic phase of BW disappeared, perhaps because of the introduction of a small amount of Cu ions, which caused a lattice distortion and thus changed the growth direction of the lattice plane. As the amount of Cu increased, the diffraction peaks moved to smaller angles, indicating that Cu ions (0.073 nm) substituted some of the W ions (0.062 nm) in the lattice [5].

Iron may be present in FeBWs in several forms, such as iron ions in the BW lattice and Fe_2O_3 or Fe_3O_4 on the surface as a result of the decomposition of $Fe(NO_3)_3$. However, peaks of Fe_2O_3 (JCPDs no. 40-1139) and Fe_3O_4 (JCPDs no. 26-1136) were not obtained from FeBWs herein. If a relatively high concentration of iron ions enters the crystal lattice during BW crystallization, then the crystal lattice will be distorted, causing a phase transition from orthorhombic to amorphous (5FeBW and 10FeBW). Notably, no FeBW exhibited any characteristic peaks of iron metal or iron oxide, probably because the iron compounds therein were amorphous. No XRD peak of iron metal was obtained, possibly because iron was doped into the lattice of BW so no peaks from iron ions or iron oxides were observed (Fig. 1). No other direct evidence of the existence of amorphous iron compounds was obtained. Conversely, Sriwichai et al. [4] postulated that the iron ions and/or the iron oxides may be loaded merely on the surface of the BW particles rather than being anchored within the lattice structure of BW.

Fig. 2 presents the FTIR spectra of prepared BW and FeBWs. All samples yielded peaks at 1072 cm^{-1}, 1384 cm^{-1}, 1620 cm^{-1} and 3420 cm^{-1}. The peak at 3420 cm^{-1} was related

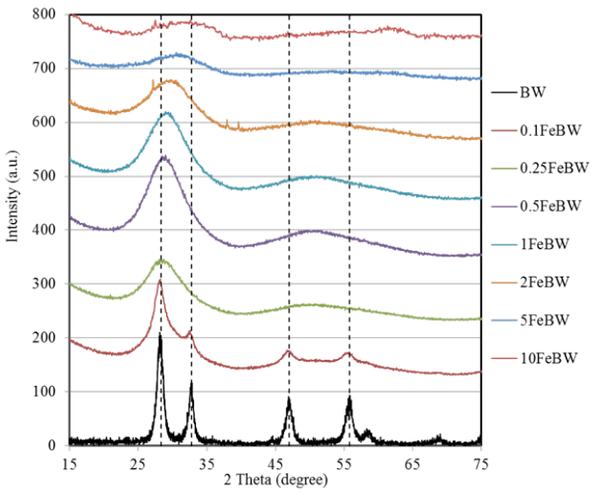

Fig. 1. XRD spectra of prepared BW and FeBWs.

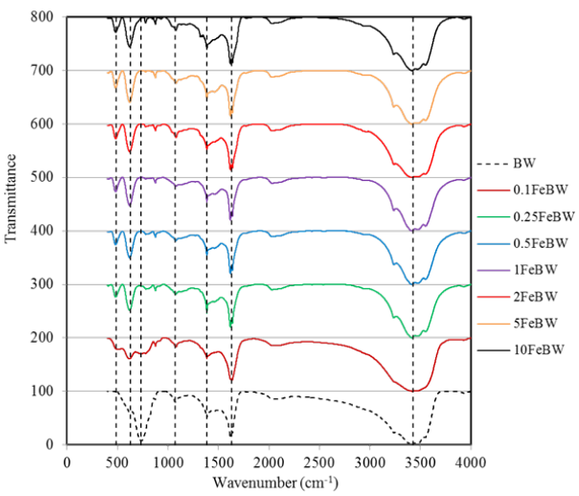

Fig. 2. FTIR spectra of prepared BW and FeBWs.

to the superposition of the vibration band of the hydroxyl groups and the stretching vibration of adsorbed water molecules. The peak at 1620 cm^{-1} is attributed to the stretching and bending vibrations of free or bonded hydroxyl groups [2,23]. Peaks at 730 cm^{-1}, 1072 cm^{-1} and 1384 cm^{-1} are assigned to the stretching vibrations of Bi-O [23,24], C-O [25] and C-H [24], respectively. FTIR bands due to Fe-O symmetric stretching vibrations are observed in the range of 620–680 cm^{-1} [26]. The peak at 489 cm^{-1} is attributed to the stretching vibrations of iron ions [27]. Only the FTIR spectra of FeBWs include iron ion (489 cm^{-1}) and Fe-O (630 cm^{-1}) peaks (Fig. 2). The weak intensities of the 1072 and 1384 cm^{-1} reveal the low adsorption of EG onto the surfaces of BW and FeBWs from the solvothermal synthetic procedure. Only pure BW yields a Bi-O (730 cm^{-1}) peak and no Bi-O peak was obtained from the FeBWs. This investigation found that iron ions substituted Bi^{3+} in FeBWs, causing the Bi-O peak to disappear.

Arakawa et al. [19] investigated the local position of Fe^{3+} in BW by making electron paramagnetic resonance measurements and performing a superposition model analysis. Their results suggested that the fact that the Fe^{3+} ion has a smaller ionic radius, 0.064 nm, than the Bi^{3+} ion, 0.096 nm, weakened the coupling of the Fe^{3+} ion to the apex oxygen, causing a deviation of the Fe^{3+} ion toward the oxygen plane of the Bi_2O_2 layers, allowing the Fe^{3+} ions to substitute Bi^{3+} ions in the Bi_2O_2 layers. Most of the iron ions were Fe^{3+} or Fe^{2+}, which were uniformly distributed on the surface of BW, and some Fe^{3+} ions substituted Bi^{3+} ions in Bi_2O_2 layers [3]. Xu et al. [6] suggested the possibility of the lattice substitution of Bi^{3+} in the $Bi_2O_2^{2+}$ by Eu^{3+} in Eu^{3+}-doped BW since the ionic radius of Eu^{3+} (0.0947 nm) is less than that of Bi^{3+} (0.103 nm). Combining FTIR results with XRD analysis, the present study further proved that some iron ions entered the lattice of BW and substituted Bi^{3+} and/or W^{6+} ions, changing the crystal structure of BW.

Table 1 lists the surface characteristics of BW and FeBWs. The BET surface areas of the FeBWs, except for 0.1 FeBW and 0.25 FeBW, exceeded that of BW. 5 FeBW had the largest BET surface area. The BET results demonstrated that doping BW with a high concentration of iron ions (Fe/W molar ratio > 0.5) increased the BET surface area. Photo catalysts with a larger surface area have more active surface sites, favoring the transport of charge carriers and, therefore, enhancing the photo catalytic performance.

Fig. 3 plots the UV-Vis absorption spectra of BW and FeBWs. The band gap is calculated by Eg = 1240/λ, where λ is the adsorption edge and Eg is the band gap. FeBWs exhibited significantly increased absorption of visible-light and exhibited a red-shifted band gap (Table 1) as the concentration of doped iron ions increased. Based on the band gap analysis, all of the FeBWs were visible-light-induced photo catalysts. A new absorption band, formed by doping with iron, might have created sub-band states in the band gap of BW, which were easily excited to generate more electron-hole pairs. Iron ions formed a new impurity level under the conduction band, reducing the energy barrier and improving the utilization efficiency of light; consequently, the band gap energy declined, in a manner similar to that which occurs upon doping with Cu [5]. The substitution of W by lower-valence cations is postulated to cause an extrinsic oxygen deficiency and improved oxide ion conductivity [28,29]. In this investigation, the most important mode involved a substitutional effect by iron ions at W^{6+} sites to form extrinsic oxygen vacancies. The oxygen vacancies are positive charge centers, at which electrons are easily bound. The excitation of electrons from such local states to the conduction band can improve absorbance of visible-light [5]. Iron-doped $CaTiO_3$ also exhibited significantly enhanced absorption of visible-light region. Yang et al. [2] found that the introduction of iron into the TiO_2 lattice can generate impurity energy levels between the conduction band and the valence band.

Fig. 4 shows SEM and TEM images of 5FeBW. 5FeBW particles exhibited significant agglomeration and were composed of rough, uneven and irregular nano particles (Fig. 4a). A further investigation was carried out using TEM to provide detailed insights into the morphology and micro structures of 5FeBW. The size of the nano particles of 5FeBW was found to be 15–30 nm (Fig. 4b).

XPS surface measurements were made to evaluate the chemical states and surface composition of 5FeBW (Fig. 5). $Bi_{4f7/2}$ and $Bi_{4f5/2}$ yielded peaks at approximately 159 and 164 eV in the Bi_{4f} region (Fig. 5a), respectively, which are attributable to Bi^{3+} in BW [30, 31]. The W_{4f} spectrum of 5FeBW exhibits binding energies of 35 eV ($W_{4f7/2}$) and 37 eV ($W_{4f5/2}$) (Fig. 5b), which correspond to W^{6+} [30, 31]. The peaks at 529.32, 529.65, 530.32, 530.98 and 531.26 eV correspond to Fe-O, Bi-O, W-O lattice oxygen, chemisorbed water and

Table 1
Surface properties of prepared BW and FeBWs

Photocatalysts	BET surface area (m^2/g)	Bandgap (eV)
BW	100.3	3.1
0.1 FeBW	86.8	2.6
0.25 FeBW	89.5	2.6
0.5 FeBW	115.2	2.4
1 FeBW	149.6	2.1
2 FeBW	191. 2	1.7
5 FeBW	236.7	1.6
10 FeBW	171.6	1.3

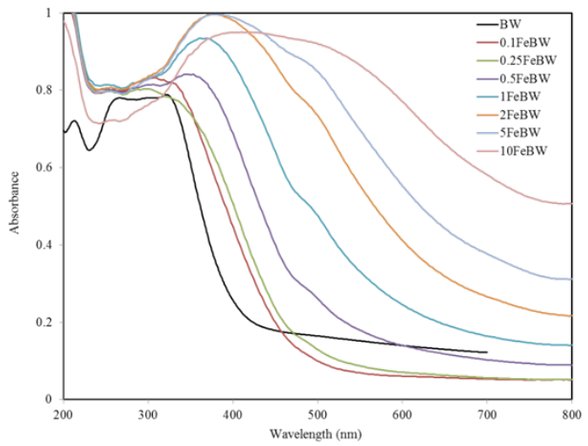

Fig. 3. UV-Vis absorption spectra of BW and FeBWs.

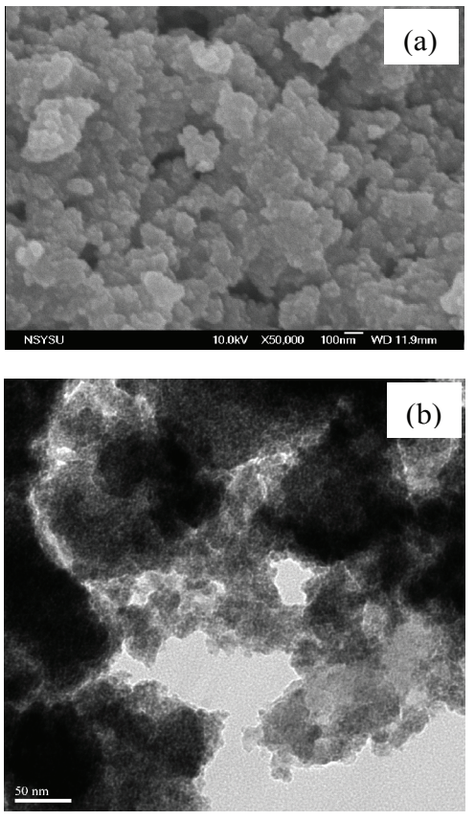

Fig. 4. Micro graphs of 5FeBW (a) SEM (b) TEM.

OH hydroxyl groups, respectively [3,32]. The peak at 529 eV corresponds to Fe-O (Fig. 5c) [33]. The peaks at 529.7 and 531.6 eV are ascribed to the Bi-O and W-O bonds in BW (Fig. 5c), respectively [30,34]. Fe^{3+} exhibits two characteristic peaks of $Fe_{2p3/2}$ and $Fe_{2p1/2}$ at 711.2 and 724.3eV, respectively (Fig. 5d). The peaks at 711.7 and 724.1 eV correspond to $Fe_{2p3/2}$ and $Fe_{2p1/2}$, respectively, suggesting that Fe was present only as Fe^{3+} [31,35]. The characteristic spin-orbit splitting of $Fe_{2p3/2}$ and $Fe_{2p1/2}$ signals is observed at approximately 710.1 and 724.4 eV, respectively, revealing that the iron species in 5FeBW were Fe^{3+} cations [11]. Fe^{2+} yielded two characteristic peaks of $Fe_{2p3/2}$ and $Fe_{2p1/2}$ at 709.8 and 722.8eV, respectively (Fig. 5d) [36]. The EG may act as both a solvent and a reductant in the solvo thermal process [37]; accordingly, Fe^{3+} was reduced to Fe^{2+}.

PL spectra are useful in determining the efficiency of charge carrier trapping, migration and transfer, which help to elucidate the fate of electron-hole pairs in a photo catalyst. Generally, a lower PL intensity suggests a lower recombination rate of photo generated electron-hole pairs, and therefore greater photo catalytic efficiency of the photo catalyst. Fig. 6 displays the PL spectra of BW and FeBWs in the range 350–550 nm. The strongest emission peak at 452 nm is attributed to the intrinsic luminescence of BW, which originates from the charge-transfer transitions between the hybrid orbital of Bi_{6s} and O_{2p} (valence band) to the empty W_{5d} orbital (conduction band) in the WO_6^{2-} complex [38]. The PL spectral intensities at 452 nm followed the order BW > 0.25FeBW > 1FeBW > 10FeBW > 0.1FeBW > 2FeBW = 5FeBW (Fig. 6). The PL spectra intensities of FeBWs are obviously reduced, suggesting a coupling effect between iron ions and BW, which was similar to that arises when

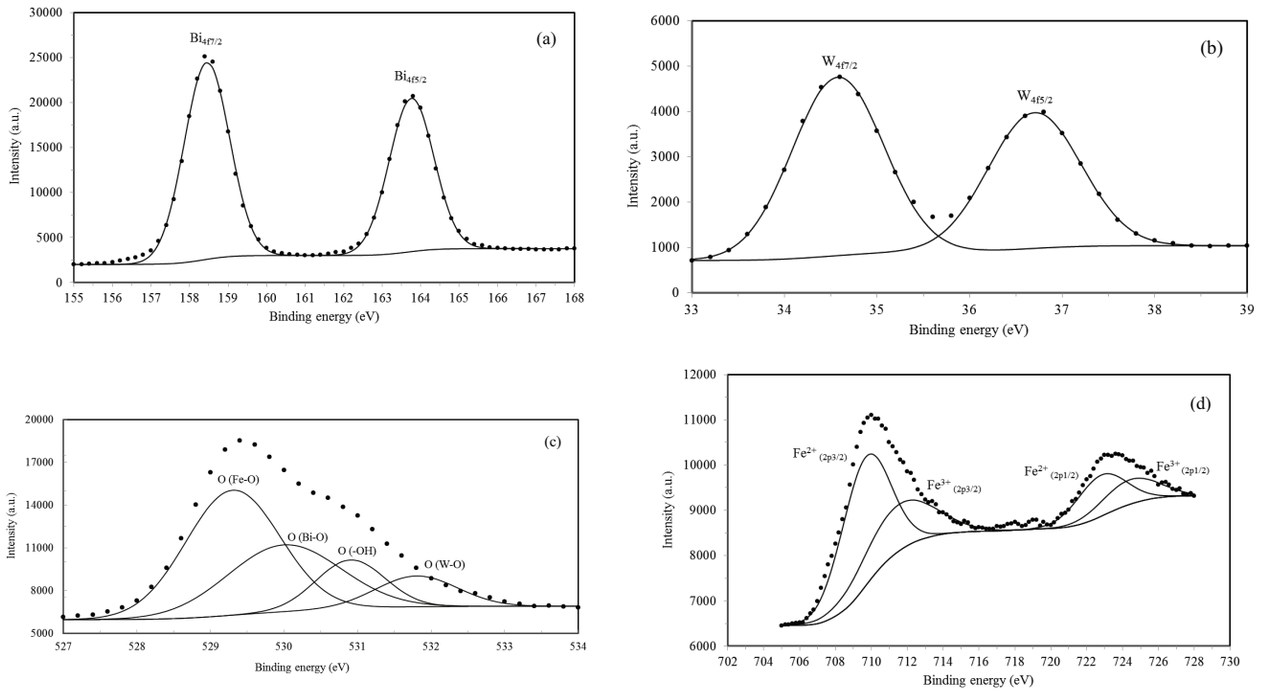

Fig. 5. XPS spectra of 5FeBW for (a) Bi_{4f}, (b) W_{4f}, (c) O_{1s}, (d) Fe_{2p}.

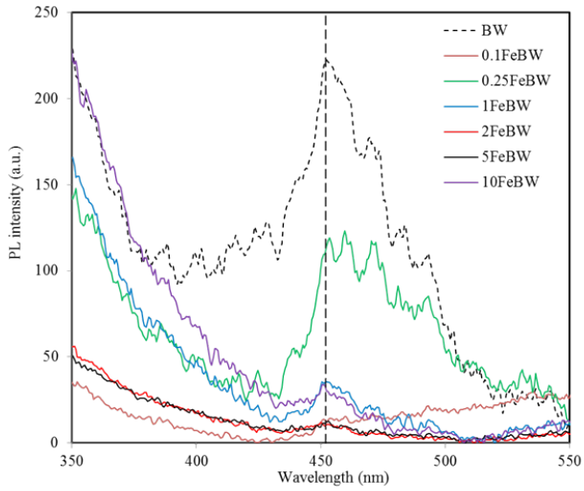

Fig. 6. PL spectra of prepared BW and FeBWs.

Fe_2O_3 [39] and iron ions [4] are doped into BW. An appropriate iron content in the BW favors the separation of the photo generated charge carriers and increases the charge carrier lifetime, improving the photo catalytic performance of FeBWs.

3.2. Comparisons of photo catalytic activity of FeBWs

Figs. 7a, 7b and 7c show the decolorization of RR2 by adsorption, solar-light photo catalysis and visible-light photo catalysis, respectively, by various FeBWs. After 60 min of reaction, the degrees of RR2 decolorization by adsorption onto BW, 0.1FeBW, 0.25FeBW, 0.5FeBW, 1FeBW, 2FeBW, 5FeBW and 10FeBW were 17%, 88%, 73%, 28%, 56%, 22%, 26% and 1%, respectively; those by solar-light photo catalysis by BW, 0.1FeBW, 0.25FeBW, 0.5FeBW, 1FeBW, 2FeBW, 5FeBW and 10FeBW were 95%, 95%, 74%, 85%, 86%, 95%, 97% and 92%, respectively; and those by visible-light photo catalysis by BW, 0.1FeBW, 0.25FeBW, 0.5FeBW, 1FeBW, 2FeBW, 5FeBW and 10FeBW were 22%, 78%, 88%, 65%, 86%, 85%, 99% and 65%, respectively. A net RR2 removal (photo catalysis - adsorption) of more than 60% was achieved when the Fe/W molar ratio exceeded unity. 5FeBW exhibited the highest efficiency of the solar-light and visible-light photo catalysis of the decolorization of RR2. The pseudo-first-order equation [Eq. (1)] was used to compare the rates of photo catalysis [40,41].

$$\ln(C/C_0) = -kt \quad (1)$$

where C_0, t and C, are the initial RR2 concentration (mg/L), reaction time, and RR2 concentration at time t (mg/L), respectively, and k is the pseudo-first-order rate constant (h^{-1}). Table 2 presents the RR2 decolorization photo catalysis rate constants of BW and FeBWs. For solar-light photo catalysis, the k values followed the order 5FeBW > 10FeBW > 0.1FeBW > BW > 1FeBW > 2FeBW > 0.5FeBW > 0.25FeBW; for visible-light photo catalysis, the k values followed the order 5FeBW > 1FeBW > 2FeBW > 0.25FeBW > 0.1FeBW > 10FeBW > 0.5FeBW > BW. Notably, 5FeBW

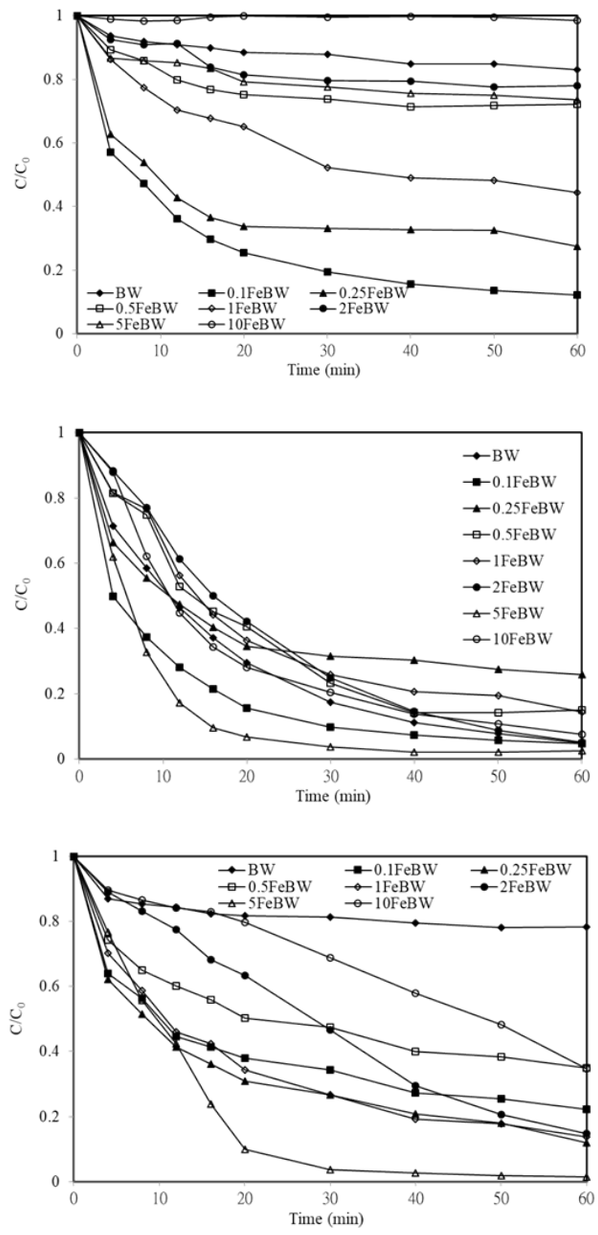

Fig. 7. Decolorization of RR2 by BW and FeBWs (a) adsorption (b) solar-light photo catalysis (c) visible-light photo catalysis ([RR2] = 20 mg/L, [photo catalyst] = 0.5 g/L, pH = 3).

exhibited the highest photo catalytic activity of all of the prepared photo catalysts; moreover, doping with iron ions increased the photo catalytic activity of BW under visible-light. Photo generated electrons in the valance band of BW are transferred directly to Fe^{3+}, resulting in the transformation of Fe^{3+} into Fe^{2+}, inhibiting the recombination of photo generated holes, prolonging the lifetime of photo generated electrons and facilitating the reduction of oxygen by the trapped electrons to generate super oxide radicals. The iron ions acted as traps of photo generated electrons and inhibited the recombination of electron-hole

Table 2
RR2 photo catalysis rate constants of prepared BW and FeBWs

	Solar-light		Visible-light	
Photo catalysts	k (h^{-1})	R^2	k (h^{-1})	R^2
BW	3.34	0.999	0.11	0.903
0.1FeBW	4.29	0.999	1.06	0.940
0.25FeBW	2.43	0.999	1.58	0.969
0.5FeBW	2.85	0.957	0.76	0.949
1FeBW	3.25	0.973	3.25	0.973
2FeBW	2.86	0.995	2.00	0.989
5FeBW	8.48	0.989	7.36	0.976
10FeBW	4.32	0.990	0.97	0.950

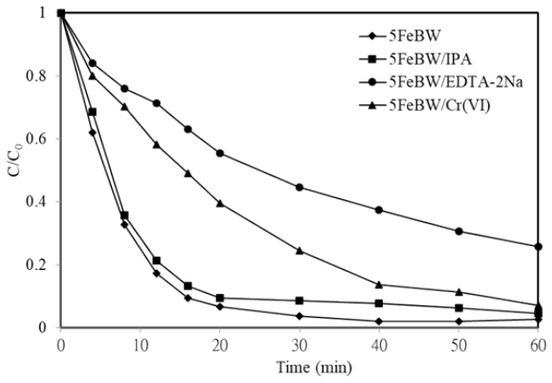

Fig. 8. Photo catalysis of RR2 in solar-light/5FeBW system in the presence of various scavengers.

pairs, which extended the lifetimes of photo generated electrons and holes. Eqs. (2) and (3) describe the involvement of Fe^{3+} and Fe^{2+}, respectively, in photo catalysis by FeBWs. The simultaneous presence of both Fe^{3+} and Fe^{2+} in 5FeBW increased the separation of photo generated electron-hole pairs.

$$Fe^{3+} + e^- \rightarrow Fe^{2+} \quad (2)$$

$$Fe^{2+} + h^+ \rightarrow Fe^{3+} \quad (3)$$

Many factors affect the photo catalytic performance of a photo catalyst; they include surface area, adsorption capacity, optical absorption and carrier recombination rate. A larger surface area typically corresponds to a smaller particle size and a higher adsorption capacity, favoring photo catalytic activity. The enhancement of the photo catalytic performance of the FeBWs herein was attributed to efficient electron-hole pair separation. The efficient electron-hole pair separation in the FeBWs system is the most important factor that affects the photo catalytic activity [4]. Guo et al. [3] reported that the iron-loaded BW shifted the absorption band into the visible-light region and the photo catalytic degradation of toluene exceeded that of pure BW. Modification with iron ions increased the rate of separation of photo generated electron-hole pairs because the iron ions acted as traps and reduced the recombination rate of photo generated electron-hole pairs.

To elucidate the mechanism of photo degradation, trapping experiments were conducted and the major active species were evaluated by using three sacrificial agents in the photo catalysis process. Cr(VI) was used as the photo generated electron scavenger to determine whether super oxide radicals were present. Cr(VI) [42], EDTA-2Na [34,43] and IPA [34,43] were utilized as super oxide radicals, holes and hydroxyl radical scavengers, respectively, to trap radicals and holes. Fig. 8 plots the photo catalysis of RR2 by the solar-light/5FeBW system in the presence of various scavengers. After 60 min of reaction under solar-light irradiation, the percentages of RR2 decolorization in the 5FeBW, 5FeBW/IPA, 5FeBW/EDTA-2Na and 5FeBW/Cr(VI) systems were 97%, 95%, 74% and 93%, respectively. The k values of the 5FeBW, 5FeBW/IPA, 5FeBW/EDTA-2Na and 5FeBW/Cr(VI) systems under solar-light irradiation were 8.48, 7.42, 1.28 and 2.66 h^{-1}, respectively. Adding EDTA-2Na effectively suppressed the photo catalytic efficiency of 5FeBW (Fig. 8), indicating that the photo generated holes were the major active species in the RR2 photo degradation process. Furthermore, the presence of Cr(VI) reduced the efficiency of RR2 degradation from 8.48 h^{-1} to 2.66 h^{-1}, suggesting that the super oxide radicals played a crucial role in photo catalytic oxidation. In contrast, adding IPA caused only minute changed in the photo catalytic activity of 5FeBW, implying that the role of the hydroxyl radicals was negligible so these radicals were not the main oxidation species in the photo degradation process. Bastami et al. [14] found that the photo generated holes were found to be the main active species in the degradation of ibuprofen by Fe_3O_4/BW nano hybrids. Zhang et al. [7] revealed that photo generated holes played an important part and hydroxyl radicals played a negligible role in the Zr^{4+}-doped BW system, as they did in 5FeBW herein.

The reusability of a photo catalyst is an important factor in determining its practical applicability. The stability and reusability of 5FeBW were investigated by performing cycling runs of the decolorization of RR2 under solar-light irradiation, as depicted in Fig. 9. Over three cycles, the proportion of RR2 that was removed by solar-light/BW at 60 min of reaction fell from 95% to 72% [44]; the corresponding decrease for solar-light/5FeBW was from 96% to 75% (Fig. 9). The photo catalytic activity of BW and 5FeBW declined over three cycles, probably because of the formation of a residual by-product of RR2 on the surface of the photo catalysts, which occupied some of their active sites. Dong et al. [45] and Qiu et al. [46] suggested that dopant Fe ions may be released into the solution after the reaction, deactivating the catalysts. Qiu et al. [46] verified the dissolution of Fe_2O_3 in eight cycles used catalyst, using TEM images. This investigation also suggested that TEM measurements could be made to verify the deactivation of catalysts. The k values of solar-light/BW in runs 1, 2 and 3 were 2.86, 1.11 and 1.09 h^{-1}, respectively [44], and those of solar-light/5FeBW in runs 1, 2 and 3 were 8.48, 2.68 and 1.24 h^{-1}, respectively. In each run, the rate of RR2 decolorization by 5FeBW exceeded that by BW under solar-light irradiation. This study suggested that doping iron ions into BW improved not only its photo catalytic activity but also its reusability.

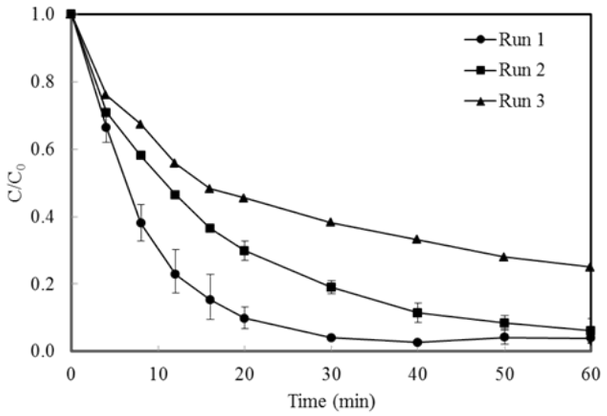

Fig. 9. Profiles of cyclic photo catalysis for RR2 in solar-light/5Fe-BW system.

4. Conclusions

In this investigation, high-performance visible-light-induced FeBWs were synthesized by the single-step solvothermal process for the first time. Iron doping inhibited grain growth and increased the surface area of BW. Some of the iron ions entered the lattice of BW and substituted Bi^{3+} and/or W^{6+} ions, altering the crystal structure of BW. FeBWs exhibited significantly increased absorption of visible-light. Photo generated electrons in the valance band of BW are transferred directly to Fe^{3+}, resulting in the transformation of Fe^{3+} into Fe^{2+}, inhibiting the recombination of photo generated holes, prolonging the lifetime of photo generated electron-hole pairs and facilitating the photo catalytic performance of FeBWs.

Acknowledgement

The authors would like to thank the National Science Council of the Republic of China, Taiwan, for financially supporting this research under Contract No. MOST 106-2221-E-151-005.

References

[1] D. Ma, S. Huang, W. Chen, S. Hu, F. Shi, K. Fan, Self-assembled three-dimensional hierarchical umbilicate Bi_2WO_6 micro spheres from nano plates: Controlled synthesis, photo catalytic activities, and wettability, J. Phys. Chem. C., 113 (2009) 4369–4374.

[2] H. Yang, C. Han, X. Xue, Photo catalytic activity of Fe-doped $CaTiO_3$ under UV–visible light, J. Environ. Sci., 26 (2014) 1489–1495.

[3] S. Guo, X. Li, H. Wang, F. Dong, Z. Wu, Fe-ions modified mesoporous Bi_2WO_6 nano sheets with high visible light photo catalytic activity, J. Colloid. Interf. Sci., 369 (2012) 373–380.

[4] S. Sriwichai, H. Ranwongsa, K. Wetchakun, S. Phanichphant, N. Wetchakun, Effect of iron loading on the photo catalytic performance of Bi_2WO_6 photo catalyst, Super lattice. Microst., 76 (2014) 362–375.

[5] G. Tan, J. Huang, L. Zhang, H. Ren, A. Xia, An enhanced visible-light-driven photo catalyst: Conduction band control of Bi_2WO_6 crystallites by Cu ion modification, Ceram. Int., 40 (2014) 11671–11679.

[6] X. Xu, Y. Ge, B. Li, F. Fan, F. Wang, Shape evolution of Eu-doped Bi_2WO_6 and their photo catalytic properties, Mater. Res. Bull., 59 (2014) 329–336.

[7] Z. Zhang, W. Wang, E. Gao, M. Shang, J. Xu, Enhanced photo catalytic activity of Bi_2WO_6 with oxygen vacancies by zirconium doping, J. Hazard. Mater., 196 (2011) 255–262.

[8] W.T. Li, W.Z. Huang, H. Zhou, H.Y. Yin, Y.F. Zheng, X.C. Song, Synthesis and photo activity enhancement of Ba doped Bi_2WO_6 photo catalyst, Mater. Res. Bull., 64 (2015) 432–437.

[9] P. Dumrongrojthanath, T. Thongtem, A. Phuruangrat, S. Thongtem, Synthesis and characterization of hierarchical multi layered flower-like assemblies of Ag doped Bi_2WO_6 and their photo catalytic activities, Super lattices Microstruct., 64 (2013) 196–203.

[10] X.C. Song, Y.F. Zheng, R. Ma, Y.Y. Zhang, H.Y. Yin, Photo catalytic activities of Mo-doped Bi_2WO_6 three-dimensional hierarchical micro spheres, J. Hazard. Mater., 192 (2011) 186–191.

[11] C.Y. Wang, C. Bottcher, D.W. Bahnemann, J.K. Dohrmann, A comparative study of nanometer sized Fe(III)-doped TiO_2 photo catalysts: Synthesis, characterization and activity, J. Mater. Chem., 13 (2003) 2322–2329.

[12] H. Li, J. Zhang, G. Huang, S. Fu, C. Ma, B. Wang, Q. Huang, H. Liao, Hydrothermal synthesis and enhanced photo catalytic activity of hierarchical flower-like Fe-doped $BiVO_4$, Trans. Nonferrous Met. Soc. China, 27 (2017) 868–875.

[13] R. Chen, J. Lu, J. Xiao, C. Zhu, S. Peng, T. Chen, α-Fe_2O_3 supported Bi_2WO_6 for photo catalytic degradation of gaseous benzene, Solid State Sci., 71 (2017) 14–21.

[14] T.R. Bastami, A. Ahmadpour, F.A. Hekmatikar, Synthesis of Fe_3O_4/Bi_2WO_6 nano hybrid for the photo catalytic degradation of pharmaceutical ibuprofen under solar light, J. Ind. Eng. Chem., 51 (2017) 244–254.

[15] C.H. Wu, C.Y. Kuo, J.T. Wu, M.J. Hsu, T.J. Jhang, Photo degradation of C.I. Reactive Red 2 in the Bi_2WO_6 system: Determination of surface characteristics and photo catalytic activities of Bi_2WO_6, React. Kinet. Mech. Catal., 117 (2016) 391–404.

[16] M. Su, C. He, V.K. Sharma, M.A. Asi, D. Xia, X.Z. Li, H. Deng, Y. Xiong, Mesoporous zinc ferrite: synthesis, characterization, and photo catalytic activity with H_2O_2/visible light, J. Hazard. Mater., 211–212 (2012) 95–103.

[17] Y.M. Wu, M.Y. Xing, J.L. Zhang, Effective visible light-active boron and carbon modified TiO_2 photo catalyst for degradation of organic pollutant, Appl. Catal. B: Environ., 97 (2010) 182–189.

[18] Y. Liu, W. Wang, Z. Fu, H. Wang, Y. Wang, J. Zhang, Nest-like structures of Sr doped Bi_2WO_6: Synthesis and enhanced photo catalytic properties, Mater. Sci. Eng. B, 176 (2011) 1264–1270.

[19] M. Arakawa, T. Hirose, H. Takeuchi, EPR study of local position for Fe^{3+} in layer oxide Bi_2WO_6, J. Phys. Soc. Jpn., 60 (1991) 4319–4325.

[20] Z. Li, W. Shen, W. He, X. Zu, Effect of Fe-doped TiO_2 nano particle derived from modified hydrothermal process on the photo catalytic degradation performance on methylene blue, J. Hazard. Mater., 155 (2008) 590–594.

[21] Y. Zhai, Y. Yin, X. Liu, Y. Li, J. Wang, C. Liu, G. Bian, Novel magnetically separable $BiVO_4/Fe_3O_4$ photo catalyst: Synthesis and photo catalytic performance under visible-light irradiation, Mater. Res. Bull., 89 (2017) 297–306.

[22] J. Zhang, H. Cui, J. Zhai, Synthesis of Bi_2WO_6/fly ash cenospheres composites with enhanced photo catalytic properties, Chin. J. Inorg. Chem., 30 (2014) 2857–2862.

[23] G. Shan, Y. Fu, X. Chu, C. Chang, L. Zhu, Highly active magnetic bismuth tungstate/magnetite composite under visible light irradiation in the presence of hydrogen peroxide, J. Colloid Interf. Sci., 444 (2015) 123–131.

[24] P. Tang, H. Chen, F. Cao, One-step preparation of bismuth tungstate nano disks with visible light photo catalytic activity, Mater. Lett., 68 (2012) 171–173.

[25] Y.L. Min, K. Zhang, Y.C. Chen, Y.G. Zhang, Enhanced photo catalytic performance of Bi_2WO_6 by graphene supporter as charge transfer channel, Sep. Purif. Technol., 86 (2012) 98–105.

[26] D. Vernekar, D. Jagadeesan, Tunable acid-base bifunctional catalytic activity of FeOOH in an orthogonal tandem reaction, Catal. Sci. Technol., 5 (2015) 4029–4038.
[27] Z.S. Liu, B.T. Wu, D.G. Yin, Y.B. Zhu, L.G. Wang, Enhanced photo catalytic activity in Al-substituted $Bi_2Fe_4O_9$ sub micro crystals, J. Mater. Sci., 47 (2012) 6777–6783.
[28] V. Sharma, A.K. Shukla, J. Gopalakrishman, $Bi_2W_{1-x}Cu_xO_{6-x}$ ($0.7 \le x \le 0.8$): a new oxide-ion conductor, J. Mater. Chem., 4 (1994) 703–705.
[29] M.S. Islam, S. Lazure, R.N. Vannier, G. Nowogrocki, G. Mairesse, Structural and computational studies of Bi_2WO_6 based oxygen ion conductors, J. Mater. Chem., 8 (1998) 655–660.
[30] Z.Q. Li, X.T. Chen, Z.L. Xue, Microwave-assisted synthesis and photo catalytic properties of flower-like Bi_2WO_6 and Bi_2O_3-Bi_2WO_6 composite, J. Colloid Interf. Sci., 394 (2013) 69–77.
[31] S. Chaiwichian, K. Wetchakun, W. Kangwansupamonkon, N. Wetchakun, Novel visible-light-driven $BiFeO_3$-Bi_2WO_6 nano composites toward degradation of dyes, J. Photo chem. Photo biol. A: Chem., 349 (2017) 183–192.
[32] D. Wang, Y. Zhen, G. Xue, F. Fu, X. Liu, D. Li, Synthesis of mesoporous Bi_2WO_6 architectures and their gas sensitivity to ethanol, J. Mater. Chem. C., 1 (2013) 4153–4162.
[33] M.J. Palimi, M. Rostami, M. Mahdavian, B. Ramezanzadeh, Surface modification of Fe_2O_3 nano particles with 3-aminopropyltrimethoxysilane (APTMS): An attempt to investigate surface treatment on surface chemistry and mechanical properties of polyurethane/Fe_2O_3 nano composites, Appl. Surf. Sci., 320 (2014), 60–72.
[34] M.S. Gui, W.D. Zhang, Q.X. Su, C.H. Chen, Preparation and visible light photo catalytic activity of Bi_2O_3/Bi_2WO_6 heterojunction photo catalysts, J. Solid State Chem., 184 (2011) 1977–1982.
[35] L. Zhang, Z. Wu, L. Chen, L. Zhang, X. Li, H. Xu, Preparation of magnetic Fe_3O_4/TiO_2/Ag composite micro spheres with enhanced photo catalytic activity, Solid. State Sci., 52 (2016) 42–48.
[36] Q. Wu, G. Wu, L. Wang, W. Hu, H Wu., Facile synthesis and optical properties of prussian blue micro cubes and hollow Fe_2O_3 micro boxes, Mater. Sci. Semicond. Process., 30 (2015) 476–481.
[37] L. Wu, J. Bi, X. Wang, X. Fu, Rapid preparation of Bi_2WO_6 photo catalyst with nano sheet morphology via microwave-assisted solvo thermal synthesis, Catal. Today, 131 (2008) 15–20.
[38] C.Y. Kuo, C.H. Wu, M.J. Hsu, Single-step solvo thermal synthesis of boron-doped Bi_2WO_6 visible-light-induced photo catalyst and determination of surface characteristics and photo catalytic activities, Desal. Water Treat., 81 (2017) 209–215.
[39] Q.S. Wu, Y. Feng, G.Y. Zhang, Y.Q. Sun, Y.Y. Xu, D.Z. Gao, α-Fe_2O_3 modified Bi_2WO_6 flower-like mesostructures with enhanced photo catalytic performance, Mater. Res. Bull., 49 (2014) 440–447.
[40] C.H. Wu, C.Y. Kuo, S.T. Chen, Synergistic effects between TiO_2 and carbon nanotubes (CNTs) in TiO_2/CNTs system under visible light irradiation, Environ. Technol., 34 (2013) 2513–2519.
[41] L. Yue, S. Wang, G. Shan, W. Wu, L. Qiang, L. Zhu, Novel MWNTs-Bi_2WO_6 composites with enhanced simulated solar photo activity toward adsorbed and free tetracycline in water, Appl. Catal. B: Environ., 176–177 (2015) 11–19.
[42] Y. Chen, S. Yang, K. Wang, L. Lou, Role of primary active species and TiO_2 surface characteristic in UV-illuminated photo degradation of Acid Orange 7, J. Photo chem. Photo biol. A: Chem., 172 (2005) 47–54.
[43] H. Huang, K. Liu, K. Chen, Y. Zhang, Y. Zhang, S. Wang, Ce and F comodification on the crystal structure and enhanced photo catalytic activity of Bi_2WO_6 photo catalyst under visible light irradiation, J. Phys. Chem. C., 118 (2014) 14379–14387.
[44] C.Y. Kuo, C.H. Wu, M.J. Hsu, Solvothermal synthesis of carbon nanotubes/Bi_2WO_6 composites to improve photo catalytic activity of Bi_2WO_6, Desal. Water Treat., 106 (2018) 116–124.
[45] C. Dong, J. Lu, B. Qiu, B. Shen, M. Xing, J. Zhang, Developing stretchable and graphene-oxide-based hydrogel for the removal of organic pollutants and metal ions, Appl. Catal. B: Environ., 222 (2018) 146–156.
[46] B. Qiu, M. Xing, J. Zhang, Stöber-like method to synthesize ultralight, porous, stretchable Fe_2O_3/graphene aerogels for excellent photo-Fenton reaction and electrochemical capacitors, J. Mater. Chem. A., 3 (2015) 12820–12827.